Synthesis of k-th Order Fault-Tolerant Kinematically Redundant Manipulator Designs using Relative Kinematic Isotropy

Frank L. Hammond III*

School of Engineering and Applied Sciences
Harvard University
Cambridge, MA, USA 02138
Email: fhammond@seas.harvard.edu
*Corresponding Author

Abstract: Fault tolerance has become an essential capability in manipulator design methodologies as robotic manipulation systems are more frequently employed in hazardous environments and on geometrically complex or heavy duty industrial operations, where mechanical joint failures are likely to occur. This work focuses on the development of a redundant manipulator design methodology aimed at minimizing the degradation in manipulator performance quality that results from *k* arbitrary joint failures. The relative weighted global isotropy index (RWGII) is developed for use as a manipulator design fitness metric. This metric takes into account the primary manipulation goal of maintaining kinematic dexterity, the secondary goals of collision avoidance and torque minimization, and fault tolerance capability. The genetic algorithm search of an immense manipulator design space, conducted using the new fault-tolerant manipulator design fitness metric, yields redundant manipulator designs that effectively minimize fault susceptibility due to *k* joint failures while maintaining dexterous, redundancy-resolved motion on specific tasks.

Keywords: kinematic redundancy; dynamics; kinematics; optimization; weighted isotropy; manipulability; constrained optimization; fault tolerance.

Biographical notes: Frank L. Hammond III is a Postdoctoral Research Fellow in the School of Engineering and Applied Science at Harvard University. He earned a Doctorate degree in Mechanical Engineering from Carnegie Mellon University, and master's degrees in Mechanical and Electrical engineering from the University of Pennsylvania. His research interests include manipulator design optimization, advanced mechatronics, biomedical engineering, and medical device development. His work has been published in several, international conferences and journals on both engineering and medical science.

1 Introduction

Fault tolerance is an important aspect of robotic manipulator design, as mechanical joint failures can have significant, adverse impacts on task performance. Fault tolerance is particularly important when designing manipulators for employment in harsh environments or on mechanically demanding tasks, which tend to exacerbate the incidence of mechanical failure. Conventional, non-redundant manipulators, those having six or fewer kinematic degrees of freedom (DOF), are generally considered fault-

intolerant because joint failures often result in a catastrophic and irrevocable loss of end-effector control. Kinematically redundant manipulators are less susceptible to these failures than non-redundant manipulators because their increased number of degrees of freedom and larger kinematic configuration spaces afford the motion flexibility necessary to implement fault compensation measures. The ability of redundant manipulators to sustain acceptable levels of performance in the presence of joint failures is not innate, however, and is heavily dependent upon certain design features and control implements.

Prior research efforts have availed several distinct methods of treating fault-tolerant manipulation, including the design and analysis failure detection frameworks (Groom, Maciejewski, and Balakrishnan, 1999), the measurement and characterization of local fault tolerant manipulator postures (English and Maciewjewski, 1998), and fault-tolerant manipulator control through redundancy resolution (Caldwell and Roberts, 2002). These control-based fault-tolerance treatments have proven very effective in enhancing the capability of redundant manipulators to mitigate and withstand various mechanical failures, but are limited in their degree of efficacy and generality by manipulator kinematic structure and morphological design. By employing the appropriate design methodology, however, redundant manipulators can be optimised to more effectively handle joint failures, locked-joint immobilizations in particular, by minimizing or preventing the degradation of manipulator performance resulting from these failures.

This work describes the development of a design methodology aimed at improving the fault-tolerance capabilities of kinematically redundant manipulators over specific, predetermined sets of tasks. As part of this methodology, a novel fault-tolerant manipulator design fitness metric, based on the concept of weighted global kinematic isotropy, is developed for use as a criterion in fault-tolerant manipulator design optimisation. This measure takes into account the primary manipulation goal of maintaining kinematic dexterity, the secondary manipulation goals of collision avoidance and torque minimization, and the degree of kinematic dexterity retained after joint failures. Using the new fault-tolerant manipulator design fitness metric as an objective function, a prescribed design space is searched to synthesize redundant manipulator designs that minimize or eliminate fault susceptibility due to k joint failures while promoting dexterous, redundancy-resolved motion for a specified set of tasks.

2 Previous work on manipulator performance and design fitness measurement

The optimisation of manipulator design fitness has been studied at great length, with much of the early work focused on the achievement of primary manipulation goals such as kinematic dexterity (Yoshikawa, 1985), kinematic isotropy (Kim and Khosla, 1991), and singularity avoidance (Stocco et al., 1998; Khan and Angeles, 2006). Many of the metrics used to quantify the achievement of these manipulation goals are based on the manipulator Jacobian matrix $\mathbf{J}(\boldsymbol{\theta})$ (Spong et al., 2005), which for an n-DOF serial manipulator maps an nx1 joint rate vector $\boldsymbol{\theta}$ to a 6x1 Cartesian end-effector velocity vector x, shown in equation (1). Because these metrics, described in Table 1, are explicit functions of a joint space to task space mapping, they are particularly useful for controlling manipulator end-effector mobility and motion quality.

$$\mathbf{J}(\boldsymbol{\theta})\dot{\boldsymbol{\theta}} = \begin{bmatrix} \mathbf{J}_{\upsilon} \\ \mathbf{J}_{\omega} \end{bmatrix} \dot{\boldsymbol{\theta}} = \begin{bmatrix} z_0 \times o_o & z_1 \times o_1 & \cdots & z_n \times o_n \\ z_0 & z_1 & \cdots & z_n \end{bmatrix} \dot{\boldsymbol{\theta}} = \dot{\mathbf{x}} \tag{1}$$

However, because they cannot consider the constraints placed on a manipulator by its actuation specifications, joint limits, and task-related manipulation goals, including fault tolerance, pure dexterity metrics are unfit for redundant manipulator performance assessment, especially on complicated tasks or in hazardous environments.

More recent research efforts (Hammond and Shimada, 2009; Hammond and Shimada, 2010) incorporate secondary manipulation goals, such as obstacle avoidance and torque minimization, into the formulation of dexterity-based design fitness metrics by factoring penalty functions into existing measures of kinematic isotropy and global kinematic isotropy. These weighted isotropy measures are well-suited to the measurement of manipulator performance on tasks involving heavy use of redundancy resolution, and have proven effective in enhancing the utility and versatility of redundant manipulators on a variety of complex tasks. However, these multiobjective measures inherently assume nominal manipulator operating conditions, and thus lack the machinery necessary to consider fault tolerance in the assessment manipulator performance and design fitness.

In light of the limitations of current manipulator performance measures on fault-tolerance assessment, a central goal of this work is to develop a metric that quantifies both the nominal performance of a redundant manipulator and the relative reduction in performance given k arbitrary joint failures. Minimizing relative performance degradation for a given manipulator design will, in theory, minimize its failure susceptibility, thereby increasing the likelihood that the manipulator sustains adequate kinematic dexterity and redundancy for a prescribed set of tasks, in the event of multiple joint faults. The following section deals with the formulation of such a metric.

3 Development of a fault-tolerant manipulator design fitness metric

3.1 Formal definition of fault tolerance

The property of fault tolerance can be assigned to several different components of a manipulation system, from the controller and its failure detection framework (Ting, Tosunoglu, and Fernandez, 1994) to the postures that a manipulator assumes during a particular motion (Roberts and Maciewjewski, 1996). In this study, we assign the property of fault tolerance to a manipulator's morphology and system actuation architecture, and we quantify the effect of the morphology and actuation specifications on the quality of global task performance.

In developing our fault tolerant manipulator design methodology, we will adopt the following definitions and properties from the work of Paredis and Khosla (1994):

1 Fault tolerant manipulator: An n-DOF manipulator that has the capacity to complete a task to specifications if one or more arbitrary joints fail.

2 k-Reduced order derivative: When k joints fail, the manipulator is reduced to (n-k) DOFs. The resulting manipulator is called a k-reduced order derivative.

3 Order of tolerance: A manipulator is k-th order tolerant if and only if all possible k-reduce order derivatives can perform the intended task.

We define optimality, within the framework of the aforementioned conventions, as the condition in which a kinematically redundant manipulator or manipulation system is k-th order fault tolerant, such that both primary and secondary manipulation objectives can be

met, without significant loss of kinematic dexterity, in the event of any arbitrary k joint failures. All joint failures considered in the study are of the locked-joint type, where joints are completely immobilized after faults occur.

Table 1 Comparison of previous kinematic dexterity and design fitness metrics

Design Metric (Researcher)	*Formulation*	*Applications and characteristics*
μ : Manipulability (Yoshikawa, 1985)	$\mu = \sqrt{\det(\mathbf{J}(\theta)\mathbf{J}(\theta)^{\mathbf{T}})}$	Measures kinematic dexterity, configuration-specific, no redundancy resolution
C : Matrix condition number (Klein and Blaho, 1987)	$C = \frac{\sigma_{max}}{\sigma_{min}} = \sqrt{\frac{\lambda_1}{\lambda_2}}$	Jacobian invertibility, proximity to kinematic singularities, scale-independent
Δ : Kinematic isotropy (Kim and Khosla, 1991)	$\Delta = \frac{M}{\Psi} = \frac{\sqrt[m]{\det(\mathbf{J}(\theta)\mathbf{J}(\theta)^{\mathbf{T}})}}{\left(\frac{\mathrm{trace}(\mathbf{J}(\theta)\mathbf{J}(\theta)^{\mathbf{T}})}{\mathrm{order}\ m}\right)}$	Measures kinematic dexterity, configuration-specific, scale-independent, no redundancy
GII : Global Isotropy Index (Stocco et al. 1998)	$\mathrm{GII} = \max_{\mathbf{W}_{\mathrm{space}}}^{\min} \frac{\sigma_{\min}[\mathbf{J}(\theta)]}{\sigma_{\max}[\mathbf{J}(\theta)]}$	Global dexterity measurement, scale-independent, no redundancy resolution
MWGII : Multiobjective GII (Hammond and Shimada, 2010)	$\max_{\mathbf{W}_{\mathrm{space}}}^{\min} \frac{\sigma_{\min}\sqrt{(\mathbf{J}(\theta)\mathbf{M}(\theta)\mathbf{J}(\theta)^{\mathbf{T}})}}{\sigma_{\max}\sqrt{(\mathbf{J}(\theta)\mathbf{M}(\theta)\mathbf{J}(\theta)^{\mathbf{T}})}}$	Global dexterity measurement, scale-independent, multiobjective redundancy resolution

3.2 Previous fault-tolerant manipulator design methods

A few methods already exist for the quantification of performance degradation in the event of locked-joint failures. One method, developed by Maciejewski (1990), calculates posture-specific fault tolerance by way of relative manipulability index $r_k(\theta)$, shown in (2). This metric defines performance loss the manipulability ratio of a rank-reduced (n-k) column Jacobian $\mathbf{J}_k$ and the full manipulator Jacobian $\mathbf{J}$, where in $\mathbf{J}_k$ the columns corresponding to the k locked-joints have been culled (3).

$$r_k(\boldsymbol{\theta}) = \frac{\mu(\mathbf{J}_k)}{\mu(\mathbf{J})};\ \mu(\mathbf{J}) \neq 0 \tag{2}$$

$$\mathbf{J}_k = \begin{bmatrix} \mathbf{J}_{v_1} & \mathbf{J}_{v_2} & \cdots & \mathbf{J}_{v_{k-1}} & \mathbf{J}_{v_{k+1}} & \cdots & \mathbf{J}_{v_{n-k}} \\ \mathbf{J}_{\omega_1} & \mathbf{J}_{\omega_2} & \cdots & \mathbf{J}_{\omega_{k-1}} & \mathbf{J}_{\omega_{k+1}} & \cdots & \mathbf{J}_{\omega_{n-k}} \end{bmatrix} \tag{3}$$

Figure 1 illustrates the concept of relative manipulability by contrasting the nominal manipulability of an 11-DOF manipulator (the larger, light-colored ellipsoid), with the manipulability of same manipulator in an identical configuration, but with three joints locked (the darker ellipsoid). Designing a manipulator for high relative manipulability ensures that faults occurring during a task have minimal impact on kinematic dexterity, thus mitigating the degree of performance degradation.

Another method, developed by Paredis and Khosla (1994), maps fault-tolerant task requirements onto manipulator designs by forcing a given manipulator to span desired workspace after sustaining joint failures. In this method, fault-tolerant designs are

developed by minimizing a penalty function which discriminates against manipulators that result in joint limit violations or range of motion deficiencies. While the task mapping method ensures that candidate manipulator designs obey physical motion constraints, it does not inherently promote improvements in manipulator dexterity. Furthermore, neither task mapping nor relative manipulability considers collision avoidance or dynamic motion constraints. Therefore, these existing methods would not be appropriate for use in fault-tolerant, redundant manipulator design optimization.

Figure 1 Graphical representation of a loss in manipulability due to the failure of three of a 12DOF manipulator's revolute joints. The outer ellipsoids represent manipulability before failure, and inner ellipsoids represent the reduced manipulability after failure. The manipulability ellipsoids show increased kinematic isotropy after several joint failures, giving a false indication of improved performance after fault occurrence.

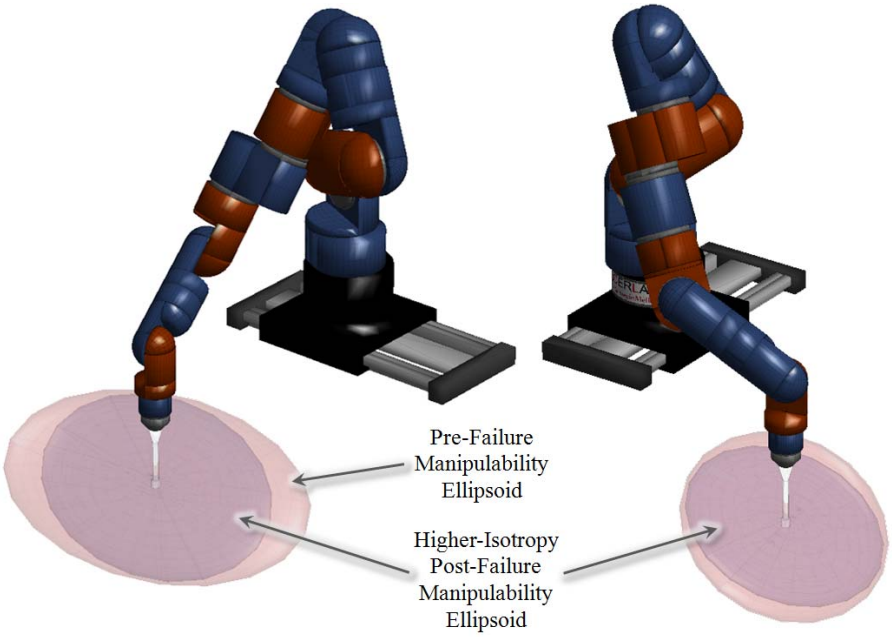

3.3 Issues with shape-based dexterity measures as a basis for fault-tolerant design

Based upon the efficacy of previous weighted isotropy-based design optimization studies (Hammond and Shimada, 2010) and inspired by the concept of Maciejewski's relative manipulability measure, the author's first attempt at a fault tolerant redundant manipulator design metric resulted in the relative weighted isotropy index $RWGII_k$ (4).

$$RWGII_k = \frac{MWGII_k}{MWGII}; \quad MWGII \neq 0 \tag{4}$$

This metric, rather than quantifying configuration-specific performance loss through the ratio of *k*-th order failure-case and nominal manipulabilities, was designed to quantify global performance degradation by the ratio of the *k*-th order failure-case MWGII, called $MWGII_k$, to the nominal MWGII value.

However, unlike relative manipulability, the proposed MWGII-based relative weighted isotropy metric is the ratio of two shaped-based, scale-independent measures which provide information about the directionality of velocity transmission, but which provide no information about the magnitude of transmission. It is, therefore, possible for a fully functional manipulator and a faulty manipulator to have identical global isotropy measures, symbolizing equivalent levels of motion transmission evenness and, by inference, equivalent kinematic dexterity, but to also have markedly different levels of motion transmission (5).

$$GII = \frac{\sigma_{\min}(\mathbf{J}_1)}{\sigma_{\max}(\mathbf{J}_1)} = \frac{\sigma_{\min}(\mathbf{J}_2)}{\sigma_{\max}(\mathbf{J}_2)}; \quad \forall \begin{cases} \sigma_{\min}(\mathbf{J}_2) = \alpha \cdot \sigma_{\min}(\mathbf{J}_1) \\ \sigma_{\max}(\mathbf{J}_2) = \alpha \cdot \sigma_{\max}(\mathbf{J}_1) \end{cases}, \quad \alpha \neq 0 \tag{5}$$

Moreover, it is also possible that joint faults can result in a more spherical manipulability ellipsoid, as shown in Figure 1. This would increase the failure-case isotropy value and produce a ratio of $MWGII_k$ to MWGII greater than one, thereby falsely indicating an improvement in system performance after joint failures. The behaviour of this proposed relative weighted isotropy metric $RWGII_k$ contradicts the intuition that a faulty manipulator cannot, by definition, be better fit for operation than a fully functional one.

The initially proposed MWGII-based relative weighted isotropy metric also suffers from the inherent marginalization of non-extrema velocity transmission ratios during the calculation of global fault tolerance. Because GII-based metric formulations consider only the global minimum and maximum velocity transmission ratios, it is possible, perhaps likely, that a manipulator with only one poor configuration along its entire motion trajectory be given a fitness value similar or equivalent to that of a manipulator which has only one desirable configuration along its entire trajectory (Fig. 2). In other words, the propensity of the manipulator to perform well on its tasks is obviated by the disparity between its best and worst case performances for GII-based measures. This property is well-suited to assessing the performance of manipulator on short motion trajectories or over small sets of manipulation tasks, but for long, complicated trajectories or large, highly disparate task sets, this property serves to prevent the assessment of both performance quality and task agility (Hammond and Shimada, 2010).

3.4 Fault-tolerant manipulator design fitness metric solution

In order to remedy the apparent deficiencies of shaped-based dexterity measures and to facilitate the optimization of multiobjective fault-tolerant manipulators, the relative weighted isotropy metric must be constructed to exhibit both scale-dependency and decreased sensitivity to manipulator performance extrema.

Sensitivity to performance extrema is decreased by factoring all velocity transmission ratios, rather than just the minimum and maximum rates, into the calculation of kinematic isotropy. In the case of spatial motion, this means that all three velocity transmission ratios, corresponding to the minor, median, and major axes of the manipulability ellipsoid, are considered. Including non-extrema velocity transmission ratios into the calculation of isotropy inherently mitigates the impact of the worse-case velocity transmission ratios and provides a more accurate and robust assessment of motion smoothness. The impact of failed manipulator joints on velocity transmission are included in isotropy by heavily penalizing, or zeroing-out, their respective columns in the Jacobian

matrix **J**, before computing the singular values of the modified Jacobian. Using these weighted singular values, kinematic isotropy is quantified by the velocity transmission ratio invariance ν, shown in (5).

$$\nu = \frac{\sqrt[(m)]{\bar{\sigma}_1 \bar{\sigma}_2 \cdots \bar{\sigma}_m}}{(\bar{\sigma}_1 + \bar{\sigma}_2 + \cdots + \bar{\sigma}_m)/(m)}; \quad m = 3 \tag{5}$$

Here, the numerator is the geometric transmission ratio mean, and the denominator is the arithmetic transmission ratio mean. In the case of global performance assessment, the velocity transmission ratio invariance function takes all velocity transmission ratios calculated over a manipulator task set comprised of *p* configurations and computes the isotropy of the entire ratio set. This provides a measure of velocity transmission ratio dispersion, and is inversely proportional to the statistical coefficient of variation measure (CV) which is defined as the ratio of a data set's standard deviation s_σ and mean σ (6).

$$CV = \frac{s_\sigma}{\bar{\sigma}} \tag{6}$$

Figure 2 Motion trajectories yielding identical GIIs but vastly disparate performance trends. The motion path on the left has several high isotropy control points and one poor isotropy point, while the right motion path contains only one high isotropy point. value because the max and min singular values come from one low isotropy point.

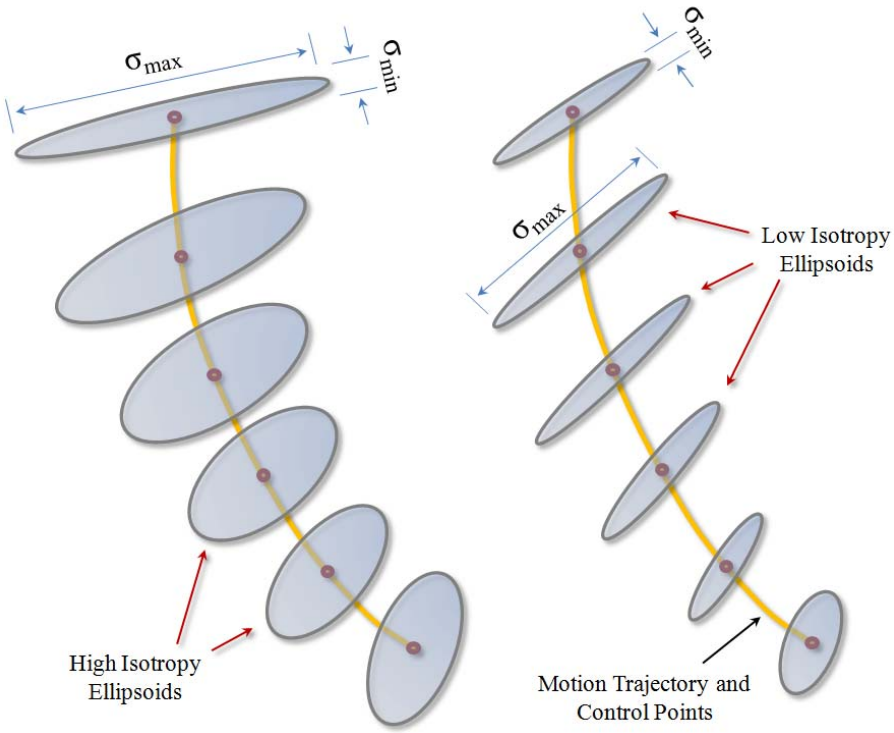

Like the GII, the maximum ν value of 1.0 denotes perfect kinematic isotropy or equivalence of velocity transmission ratio, indicating high dexterity. The minimum ν value of 0.0 indicates extreme kinematic anisotropy, or very poor velocity transmission ratio congruence. Unlike the GII, ν exhibits sensitivity to the total number of high or low isotropy configurations so that more ambiguous performance classifications, such as the one seen in Figure 2, do not occur.

Figure 3 illustrates the sensitivity of the GII and the velocity transmission ratio invariance to the occurrence of high or low transmission ratios. The initial values of GII and ν in this figure are based on the set of arbitrary velocity transmission rates {1.0, 5.0}, which yields an isotropy value of 0.2 in both cases. As additional velocity transmission rates of value 5.0 are added to the set, the GII, represented by the dashed line, shows no sensitivity to the total number of 5.0 rates, and continues to indicate a 0.2 isotropy value despite the fact the only one instance of a 1.0 transmission rate has occurred. This behavior essentially neglects the tendency of this transmission rate set to be isotropic and provides no derivatives upon which to optimize the set to improve isotropy. The velocity transmission ratio invariance, on the other hand, shows high sensitivity to the occurrence of 5.0 transmission rates, and increases its isotropy value as the occurrence of that rate increases. This behavior gives priority to performance trends rather than performance extrema, and provides derivatives which can be used for isotropy improvement.

Figure 3 Sensitivity of velocity transmission ratio invariance ν to the number of DOF. Here, we start by computing GII, ν, and CV with only two velocity transmission rates, 2 and 10, then proceed to add velocity rates of 10 to illustrate sensitivity to rate frequency.

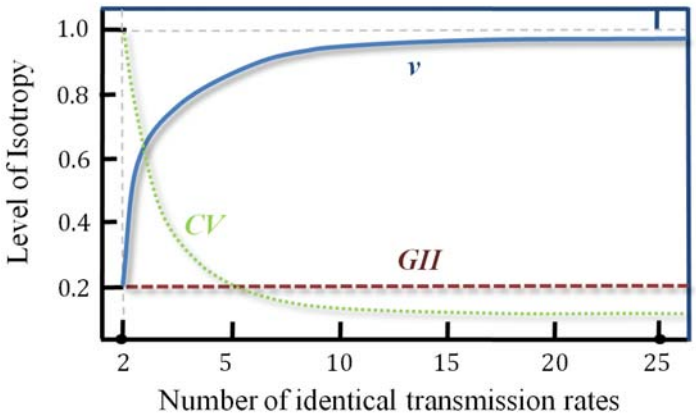

The inclusion of velocity transmission ratio magnitudes, in addition to kinematic isotropy, in relative weighted isotropy introduces the scale-dependency necessary to handle cases where the isotropy measures of nominal and degraded manipulators are very similar. Velocity transmission ratio magnitudes are incorporated into the calculation of fault tolerance fitness using the mean of the manipulability measure μ. This measure, which is similar in fashion to Yoshikawa's manipulability measure, is the defined as the product of manipulator Jacobian eigenvalue means, and likewise quantifies the ability of a manipulator to move its end effector (7).

$$\bar{\mu} = \sqrt{\bar{\lambda}_1 \bar{\lambda}_2 \ldots \bar{\lambda}_m} = \bar{\sigma}_1 \bar{\sigma}_2 \ldots \bar{\sigma}_m$$
$$\bar{\lambda}_i = \sum_{j=1}^{p} \lambda_{i,j} \tag{7}$$

Though using the eigenvalue means tend to marginalize the best and worst transmission rates for a set of p manipulator configurations, this method provides more information about overall manipulator mobility than using isotropy or velocity transmission rate invariance alone, and therefore gives a more salient indication of manipulator performance degradation.

With its two major components defined, the improved relative weighted isotropy metric is computed by taking the ratio of the mean manipulability measure and velocity transmission ratio invariance products for both the nominal manipulator and the faulty manipulator, as seen in (8).

$$RWGII_k = \frac{\bar{\mu}_k \nu_k}{\bar{\mu}\nu}; \quad \left.\begin{matrix} \bar{\mu}_k \le \bar{\mu} \\ \nu_k \le \nu \end{matrix}\right\} \ \forall\ k; \quad \bar{\mu}, \nu \neq 0 \tag{8}$$

In this equation, μ_k is the mean manipulability of the degraded manipulator and v_k is its velocity transmission ratio invariance. This new formulation of relative isotropy, unlike the rhetorically proposed MWGII-based version, guarantees that for a given configuration and a coincident locked-joint failure at that configuration, the resulting faulty manipulator cannot have a greater $\mu_k v_k$ product than its nominal counterpart, as μ_k must always be less than μ and v_k must necessarily be less than v for a known configuration, as stated in (9).

$$\left.\begin{matrix} \bar{\mu}_k \le \bar{\mu} \\ \nu_k \le \nu \end{matrix}\right\} \ \forall\ k \quad \therefore \quad RWGII_k = \frac{\bar{\mu}_k \nu_k}{\bar{\mu}\nu} \le 1 \tag{9}$$

For global fault tolerance assessment, however, this relationship cannot be guaranteed for two reasons:

1 In compensating for lost dexterity, a degraded manipulator may assume configurations that result in higher mean manipulability or lower velocity transmission rate invariance than the nominal manipulator with.

2 As more manipulator configurations are added to the $RWGII_k$ calculation, mean manipulability and velocity transmission ratio invariance vary nonlinearly and independently of one another, and simultaneously become less sensitive to changes in performance. This creates a nonlinear relationship between the ratios of degraded and nominal manipulability which can lead to $RWGII_k$ values greater one.

Despite this drawback, the $RWGII_k$ is far less sensitive to worst-case velocity transmission rates than GII-based fault-tolerance metrics and shows high sensitivity to manipulability changes, which provides additional performance contrast when kinematic isotropy for a manipulator and its degraded form are similar.

4 Fault-tolerant redundant manipulator design synthesis using $RWGII_k$

4.1 Manipulator design specification and task definition

The redundant manipulator morphology and manipulation task used in this study are based loosely upon prospective applications of robotic manipulators to aircraft inspection and repair facilities on naval warships. Such applications are situated in harsh, isolated environments and entail very complex, heavy duty, mechanically demanding tasks. Manipulators designed for these environments and tasks must have the capacity to sustain moderate damage or system failure and still maintain adequate performance, as the availability of repair service or replacement manipulators is limited. The initial design candidate is a 12DOF manipulator with a mobile, track-mounted base. The size of configuration of the morphology is based in part upon high payload industrial robots (large, powerful actuators), and in small part on low payload, high-throughput robots.

The manipulation workspace is modeled after an aircraft carrier hangar deck, where aircraft repair and inspection tasks are performed. Because the deck is very large with respect to the intended task space in this study, no physical constrains need be assigned to the task space. For the purpose of this study, we will assume that the hangar deck is populated by the 12DOF service manipulator, an armament crate and forklift, and, the target of inspection and repair, an F-14 Tomcat fighter jet (Fig. 4).

A manipulator fit for this aircraft repair and inspection operation is required to perform the following two tasks in both its nominal and degraded operating states:

1 The inspection of the aircraft fuselage, wings, and engines, which encompasses reaching a specific set of control points loosely representing location and configurations commensurate with inspection procedure.

2 An ordinance loading/unloading task in which involves the lifting and positioning of armaments, which, in this case, are air combat missiles.

It is assumed that the aircraft being repaired are rearmed is positioned within range of the manipulator's linearly actuated base, and that the manipulator only tends to one side of the aircraft, in the case the port side. Figure 4 shows the hangar bay workspace, the F-14 Tomcat fighter jet, and the positioning of the armament and assistive machinery, including an armament crate and forklift. Figure 5 illustrates the set of control points on the top surface of the aircraft which must be reached by the manipulator in order to perform aircraft inspection. Figure 6 shows both the location of inspection control points on the bottom surface of the aircraft wing and the location of the missile armaments of the F-14 Tomcat jet, the 95kg Sidewinder (smaller missile) and 150kg Phoenix (larger missile), which will be loaded/unloaded using the 12DOF service manipulator.

The inspection and armament loading tasks are not bound by temporal constraints such as maximum cycle time, as these tasks are designed for accuracy and dexterity, not throughput and work volume. Both the inspection task and missile placement task have pre-defined motion paths so that redundancy resolution only affects the joint space trajectories, and not task space trajectories.

Figure 4 Organization of the aircraft carrier hangar at the site of the aircraft to be serviced, the F-14 Tomcat jet. The 12DOF manipulator that will service the jet is mounted above on the aircraft carrier hangar ceiling.

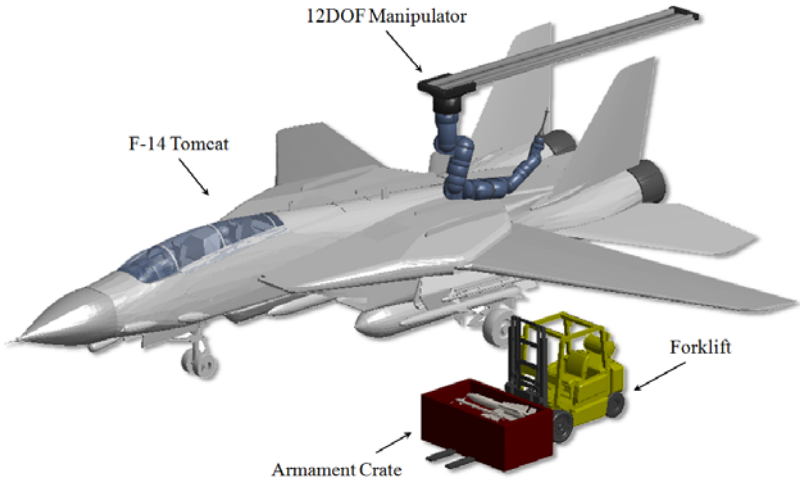

Figure 5 The positioning of control points comprising the motion path used to inspect the top surface of the port-side aircraft wings.

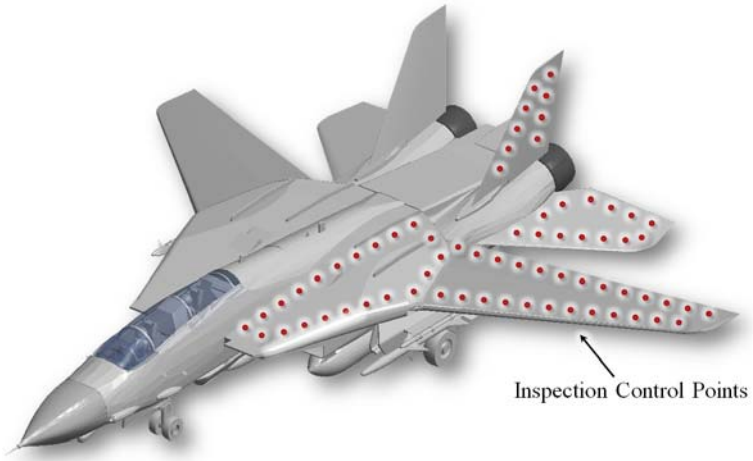

4.2 Design optimisation methodology

The synthesis of a k-th order fault-tolerant kinematically redundant manipulator is accomplished by ensuring that the worst case k-th order derivative manipulator suffers no collisions, torque or joint limit violations, or reachability issues, and by forcing the minimum isotropy above a specified threshold. Using the proposed relative weight isotropy metric and a well-formulated optimization methodology, the achievement of these performance objectives is generally tractable.

Figure 6 The relative positions of the F-14 Tomcat armaments (highlighted in dashed outlines) to be replaced by the fault-tolerant manipulator during aircraft service, and the positioning of control points comprising the motion path used to inspect the bottom surface of the port-side aircraft wings.

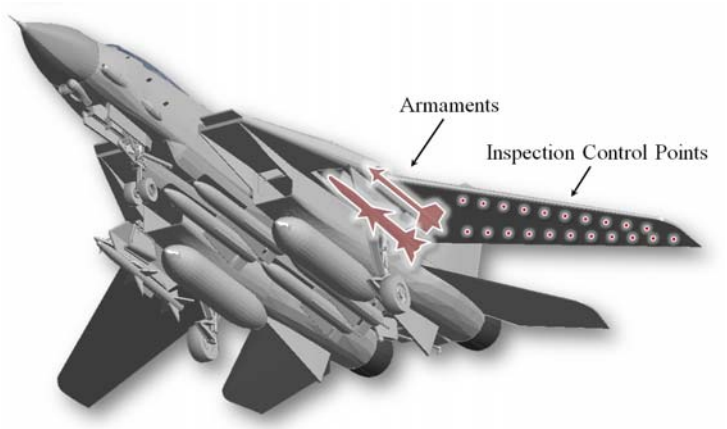

However, the degree to which a manipulator can be optimized and the computational heft of the optimization method are predicated, in large part, upon the size and complexity of both the manipulator design space, the definition of failure conditions, and the formulation of the design problem. The following describes the nature of the design space, and failure condition properties, and outlines a problem formulation that seeks to minimize computational cost and increase the likelihood of finding a near-optimal fault tolerant manipulator morphology.

4.2.1 Fault-tolerant manipulator design space description

The optimization of the aforementioned 12DOF manipulator morphology for fault-tolerance involves a design space comprised of four major morphological variable types: link type, link dimension, actuator type, and linkage assembly.

The link types available for design are shown in Fig. 7. Each link is representative of a rudimentary link shape commonly found in industrial and field robotics. Each link has a set of major dimensions, each major dimension with its own range and resolution. These dimensions and ranges essentially create a design subspace for each link, which itself can be searched during optimization to provide a more robust fault-tolerant design solution.

Each link has assigned to it one joint which contains its own actuator. Joints are limited to revolute motion only (not spherical or prismatic), but the actuation capability of each joint can be adjusted in actuator design subspace, which contains three different actuators (Fig. 8). The actuators vary proportionally in mass and maximum torque, such that greater torque capacity comes at the expense of increased mass.

The linkage assembly is a function of link type, link dimension, and joint type. The number of links used at any time in the fault-tolerant manipulator design is set to 12 for this study, but the distribution of these links along the kinematic linkage is unstructured. This creates design flexibility similar to that seen in modular design problems, where part selection is largely unconstrained. As is the case in modular manipulator design studies (Paredis and Khosla, 1993), this flexibility leads to an enormous number of linkage design permutations which typically obviates the use of exhaustive search methods.

Given the number of link types, link dimension sets and ranges, and joint design types, there are 150 total number link-joint permutations available in the link design space. The size of the manipulator design space created by this link design subspace is computed using the binomial coefficient equation (Bryant, 1993).

Figure 7 Specifications of the link types, dimensions, and dimension ranges available for fault-tolerant manipulator design.

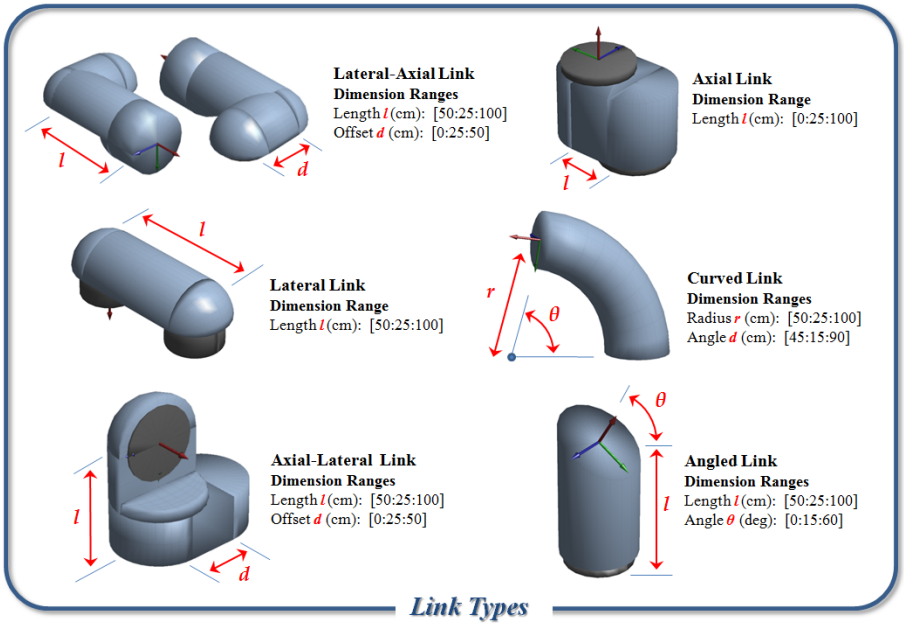

Figure 8 Specifications of the joint actuators available for fault-tolerant manipulator design.

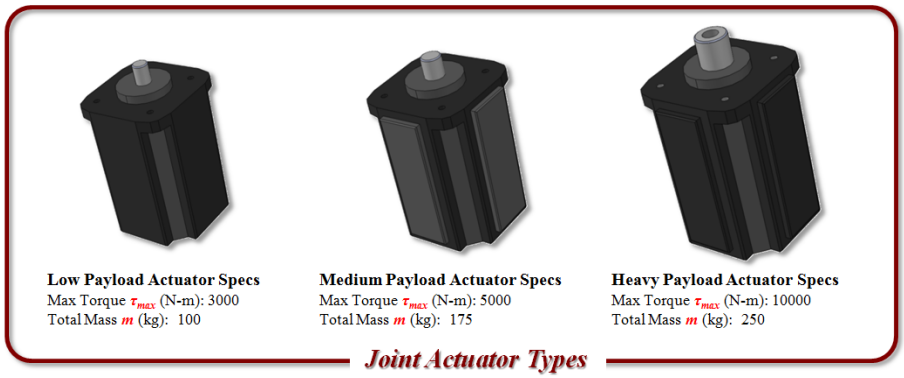

In this equation (10), n is the total number of members in a set and p is the number of members that will be selected at any one time, without regard to ordering. With n = 150 and p = 12 for a 12DOF manipulator, the total number of morphological designs in the design space is 172.74 x 10^{15}, clearly far too large a space to be searched exhaustively.

$$\binom{n}{p} = \frac{n!}{p!(n-p)!} \tag{10}$$

4.2.2 Calculating failure probability

In designing *k*-th order fault-tolerant manipulators, one must make assumptions about the likelihood of joint failure to accurately assess failure susceptibility of an entire mechanism. Many design problems warrant the assumption that each *k*-th order derivative is equally likely to occur, regardless of performance. There may, however, be instances where a designer has prior statistical knowledge of joint failure probability, or has a fault prediction formulation that avails the likelihood of a *k*-th order derivative instantiation given certain performance data. In these instances, a designer may want to factor *k*-th order derivative likelihood into the definition of fault tolerant morphological fitness, such that those derivatives which are more likely to occur are given priority during fitness measurement.

In this study, the likelihood of joint failure is predicted by the proximity of a joint's output torque to its nominal torque, and the percentage of time that the joint spends at close proximity. The likelihood of joint failure is computed by (11), where τ_{max} is the nominal torque of joint *i*, and $t_{i,j}$ is the duration of the motion of joint *i* at control point *j*, and t_{total} is the total motion time. During design optimization, the joint-link pairs with the greatest $P_{i,fail}$ value can be scrutinized more heavily.

$$P_{i,fail} = \frac{\sum_{j=1}^{m}\left(1 - \frac{\left(\tau_{\max} - \tau_{i,j}\right)}{\tau_{\max}}\right)\cdot t_i}{\left(t_{total}\right)} \tag{11}$$

4.2.3 Manipulator design optimisation algorithm

The optimization of the 12DOF 3rd order fault-tolerant manipulator is accomplished using genetic algorithms. The source code used to facilitate these algorithms is part of the MATLAB® Global Optimization Toolbox. Genetic algorithms were chosen as the optimization method because of their ability to search very large design spaces and find globally optimum solutions, regardless of the tonicity of the cost function and the number of local minima in the design space. The GA-based design optimization process consists of three major steps:

1 Creation of an initial generation of candidate manipulator designs.

2 Simulation of each design phenotype and assessment of *k*-th order tolerance, using $RWGII_k$, by systematically locking joints and quantifying performance degradation.

3 Creation of a new generation of candidate manipulators based upon elite phenotype selection, crossover, and mutation algorithms.

4.2.3.1 Populating the initial generation

The initial population of 24 manipulator design phenotypes is generated by random selection of the genes. Every 12DOF morphology in this and each successive population is represented by a 24-gene chromosome comprised of 12 link type integer genes and 12 actuator type integer genes (Fig. 9). The 12 link type integers range from 1 to 50, for the 50 different link shapes available in the design space, and the 12 actuators type range from 1 to 3, for the three actuation units available for each joint{low, medium, heavy}. The link and actuator types at a joint *i* can be changed independently of one another, such that crossover and mutation operations do not require special pairing rules for each joint.

Figure 9 The organization of fault-tolerant manipulator design chromosomes (right) with respect to the actual manipulator morphology (left).

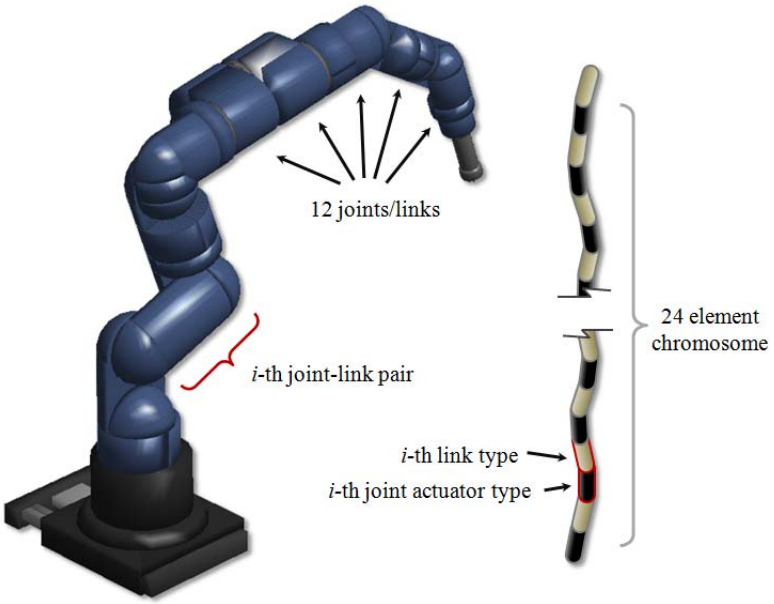

4.2.3.2 Simulating fault-tolerant manipulation tasks

The simulation of the aircraft inspection and arming tasks is performed using a velocity-based inverse kinematics solver, which include several motion control sub-algorithms ensure adherence to manipulator mechanical and actuation specifications, and to facilitate the resolution of kinematic redundancy. These algorithms include well-recognized singularity avoidance (Wampler, 1986), torque and energy minimization (Ma, 1995), and collision avoidance (Maciejewski and Klein, 1985) algorithms. The formulations used to implement these control algorithms are listed in Table 2.

4.2.3.3 Testing for k-th order fault tolerance

For every 24-phenotype generation of 12DOF manipulator designs, each candidate design is simulated once performing the aircraft inspection and arming tasks in its nominal, fully-functional state. If, in its nominal state, a manipulator violates maximum actuator

torques, suffers a collision, or is unable to reach all control points in a motion trajectory, that manipulator is immediately given a fitness score of zero, guaranteeing the elimination of its phenotype from elite phenotype selection. Should a manipulator successfully perform the task without violating any kinematic or dynamic constraints, it progresses to the next design fitness assessment for (k+1)-th order fault-tolerance which, in the first step after nominal state simulation, is 1st order fault-tolerance.

Table 2 List of theoretical bases for velocity-based redundancy-resolved inverse kinematics

Design Metric (Researcher)	*Formulation*	*Method*
Singularity avoidance (Wampler, 1986)	$\dot{\boldsymbol{\theta}} = \mathbf{J}^T(\mathbf{J}\mathbf{J}^T + \gamma_N \mathbf{I})^{-1}\dot{\mathbf{x}}, \quad \gamma_N = \lambda\left(1 - \frac{\mu}{\mu_0}\right)^2$	Null space projection
Torque Minimization (Ma, 1995)	$\boldsymbol{\tau}\left[\frac{\partial \mathbf{H}}{\partial \boldsymbol{\varphi}}\ddot{\boldsymbol{\theta}} + \ddot{\mathbf{H}}\frac{\partial \boldsymbol{\theta}}{\partial \boldsymbol{\varphi}} + \frac{\partial \mathbf{C}}{\partial \boldsymbol{\varphi}} - \frac{d}{dt}\left(\frac{\partial \mathbf{C}}{\partial \dot{\boldsymbol{\varphi}}}\right)\right] + \dot{\boldsymbol{\tau}}^+\left[2\dot{\mathbf{H}}\frac{\partial \boldsymbol{\theta}}{\partial \boldsymbol{\varphi}} - \frac{\partial \mathbf{C}}{\partial \dot{\boldsymbol{\varphi}}}\right] + \ddot{\boldsymbol{\tau}}^T\mathbf{H}\frac{\partial \boldsymbol{\theta}}{\partial \boldsymbol{\varphi}} = 0$	Null space projection
Collision Avoidance (Maciejewski and Klein, 1985)	$\dot{\boldsymbol{\theta}} = \mathbf{J}_e^+\dot{\mathbf{x}} + \sum_{i=1}^{n} \alpha_{\eta i}[\mathbf{J}_{oi}(\mathbf{I} - \mathbf{J}_e^+\mathbf{J}_e)]^+(\alpha_{oi}\dot{\mathbf{x}}_{oi} - \mathbf{J}_{oi}\mathbf{J}_e^+\dot{\mathbf{x}}_e)$	Null space projection

At each k-th order fault-tolerance assessment step, joints are stochastically selected and locked according to the likelihood of joint failure, calculated using (11). A total of 20 different k-reduced order derivative manipulators will be generated and simulated, with the design variants for each being the set of joints that are locked and the angle in which those joints are locked. If any of its k-reduced order derivatives fail to complete the task, then the design phenotype is given a zero $RWGII_k$ value and is eliminated from contention. If all k-reduced order derivatives, successfully complete the tasks, then the derivative with the lowest fitness score proceeds to the next (k+1)-th order fault-tolerance assessment step. This process repeats until either one of phenotype's k-reduced order derivatives fails to complete the tasks, or the maximum order of fault-tolerance, which is order 3 in this study, has been achieved by said phenotype.

4.2.3.4 Populating new generations

After all phenotypes in a generation are simulated and analyzed in this manner, the next generation of phenotypes is generated by elite phenotype selection, mutation, and crossover. In MATLAB-based genetic algorithm toolbox, the elite phenotype count was set to 6 children, and crossover fraction was set to 0.6 to yield 9 crossover children, and remaining 9 children were, by default, created by mutation. Stopping criteria for the genetic algorithm were a function tolerance of 1.0×10^{-12} and a maximum generation number of 2000. The complete genetic algorithm-based optimization process used to design the 12DOF 3rd order fault-tolerant manipulator is summarized in Figure 10 below.

4.2.4 Assumptions made in the optimization methodology

Several assumptions and conditions were developed during problem formulation to reduce the problem complexity while maintaining an adequate level of accuracy and robustness. The assumptions are as follows:

1 All joints are revolute with limitless motion range. Joint motion can only be impeded by obstacles or dynamics constraints.

2 Changes in link dimensions have a negligible effect on a link-actuator pairs total mass and center of mass, given that the actuators comprises a majority mass.

3 All manipulators start their motion trajectory from a completely outstretched configuration to ensure that there are no self-collisions.

Figure 10 **A** flow diagram of the fault-tolerant manipulator design algorithm.

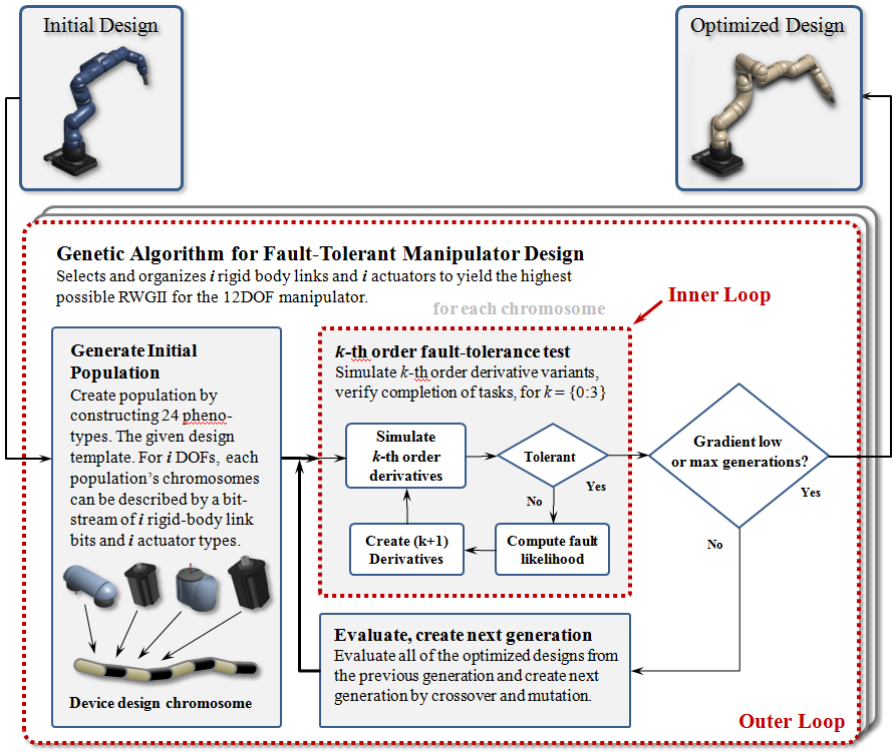

5 Design synthesis results

5.1 Simulation statistics

The genetic algorithm-based optimization of the 12DOF 3rd order fault-tolerant manipulator design, which terminated after 738 generations, resulted in 141 valid design solutions, out of 17,712 phenotypes considered. Figure 11 shows a non-monotonic but generally steady improvement in $RWGII_k$ with successive manipulator generations, as well as a steady decrease in the percentage of manipulator designs that do not meet fitness criteria. This confirms that the GA-optimization is converging on a population with a high average RWGII value as it prunes the design space of undesirable genes. There are a

few distinct, rapid increases in manipulator design fitness optimization, demarcated by the dashed vertical lines, which seem to indicate a large, advantageous change in a principle design parameter.

Figure 11 **A** plot of manipulator design fitness with respect to design generation number. The solid line (sampled every 50th generation) represents $RWGII_k$ fitness (left scale), and the dashed line represents percentage of fault-tolerant manipulator designs per generation (right scale).

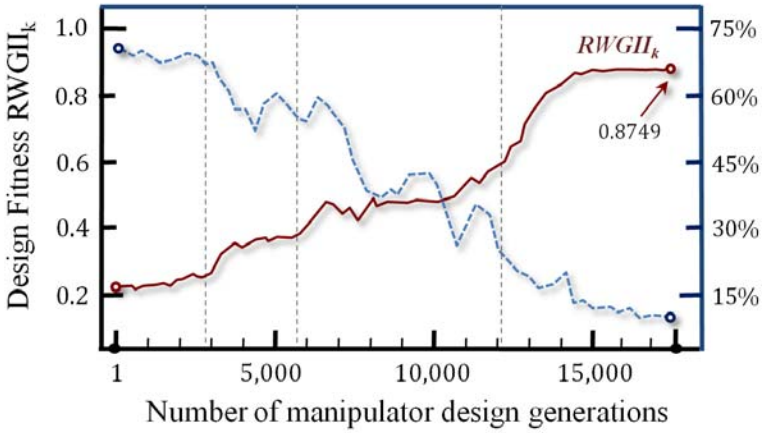

5.2 Fault-tolerant redundant manipulator solutions

Figure 12 shows the fittest 12DOF 3rd order fault-tolerant manipulator and the type of actuator selected for each joint. Figure 13 shows the fittest 12DOF 3rd order fault-tolerant manipulator and the type of actuator selected for each joint. Figures 14, 15, and 16 show the third fittest manipulator performing the tasks of airfoil inspection, missile armament retrieval, and missile armament placement, respectively. Figure 17 is a mechanical comparison of the fittest and least fit fault-tolereant manipulator design solutions.

5.3 Design solution trends and insights

The solutions generated by this optimization algorithm varied greatly in shape and overall size, but possessed a few common traits worth noting. First, the distribution of actuator types along the manipulator linkages never included small or medium actuators at the 1st or 2nd joints (the lower joint number is more proximal), and never included medium or heavy actuators at the 9th-12th joints. This trend makes intuitive sense because greater torques are needed at the proximal joints of any manipulators, and because placing large actuators in distal joints would markedly increase torque demands and, by extension, energy consumption along the rest of the manipulator linkage.

A second design solution trend worth noting is the shape and length of the links used in the manipulator linkages. Most of the valid solutions exhibited uniformity in the length of the 1st-9th manipulator links. Generally, only the distal links near the end effector were short relative to the rest of the links, and this is likely due to dexterity required to effect small changes in end-effector orientation for both the inspection and the re-arming tasks. None of the salient design solutions had shorter links at the base than at the tip, and every solution contained at least 3 links whose transformations include orientation changes (elbow, lateral-axial, axial-lateral, and angled link types).

Figure 12 An illustration of the 12DOF 3rd order fault-tolerant manipulator having the highest design fitness value.

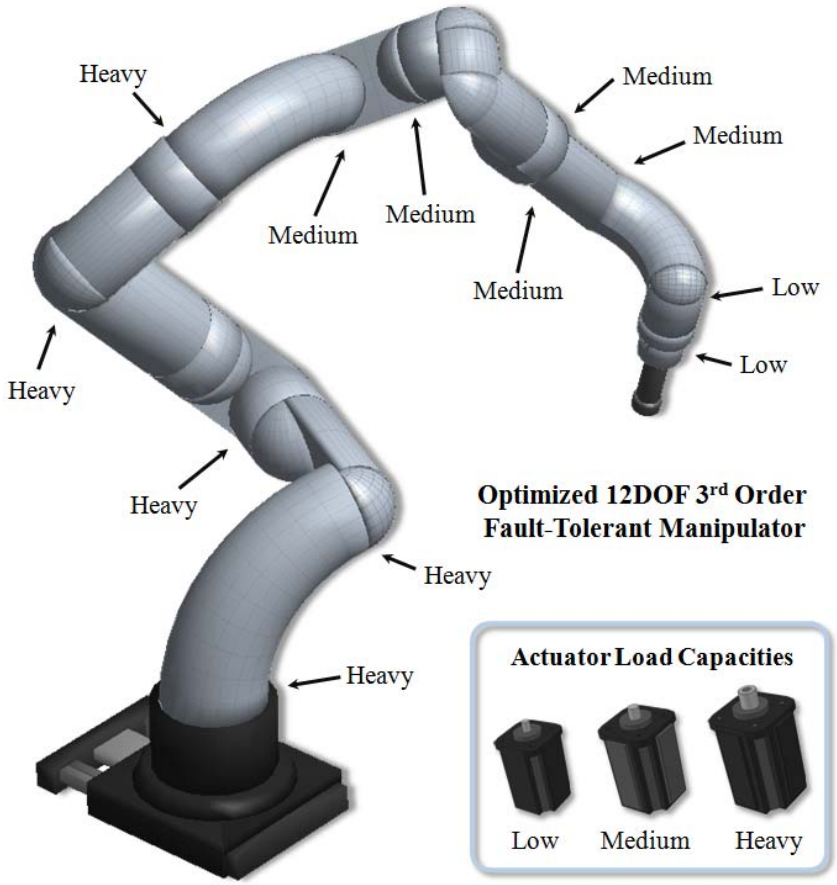

The third design solution trend worth noting concerns manipulator performance and design fitness values. The top three manipulator design solutions with respect to RWGII exhibited high dexterity and low energy consumption compared to lesser-fit design solutions, in addition to having to lowest percentage of isotropy loss (Table 3) after joint failures. The valid 3rd order fault-tolerant manipulators with the lowest $RWGII_k$ exhibited some of the lowest dexterity and highest energy consumption values, though some manipulator designs with slightly higher $RWGII_k$ had worse performance.

Figure 13 An illustration of the 12DOF 3rd order fault-tolerant manipulator having the third highest design fitness value.

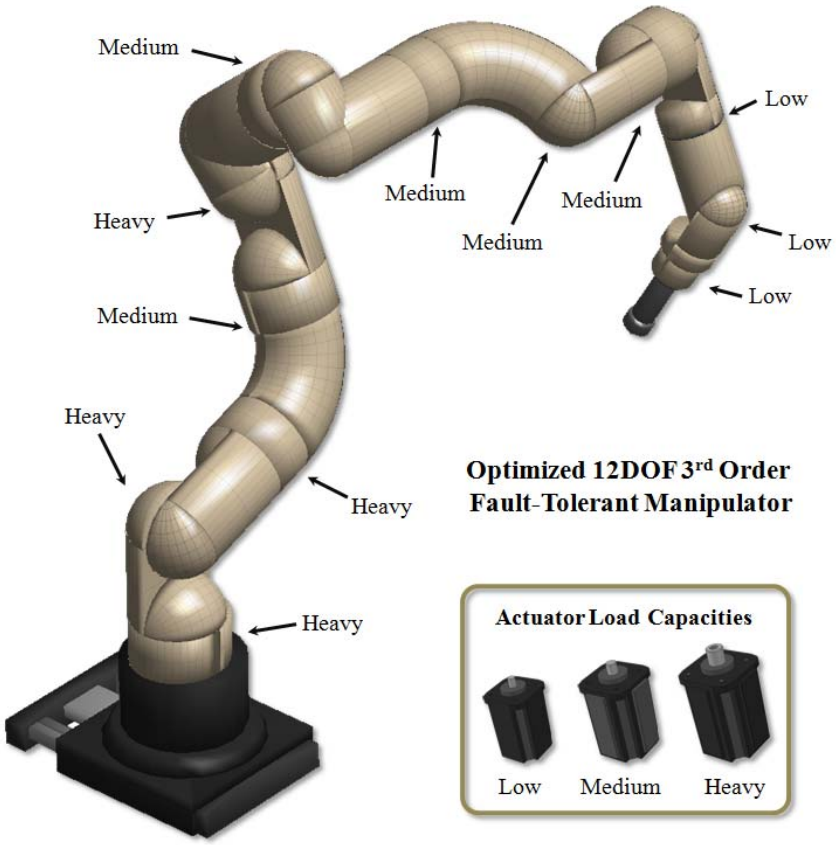

Figure 14 The third-fittest 12DOF 3rd order fault-tolerant manipulator successfully inspecting the port-side aircraft wing with 2 failed joints (contained in the highlighted links).

Figure 15 The third-fittest 12DOF 3rd order fault-tolerant manipulator successfully accessing an armament container with 2 failed joints.

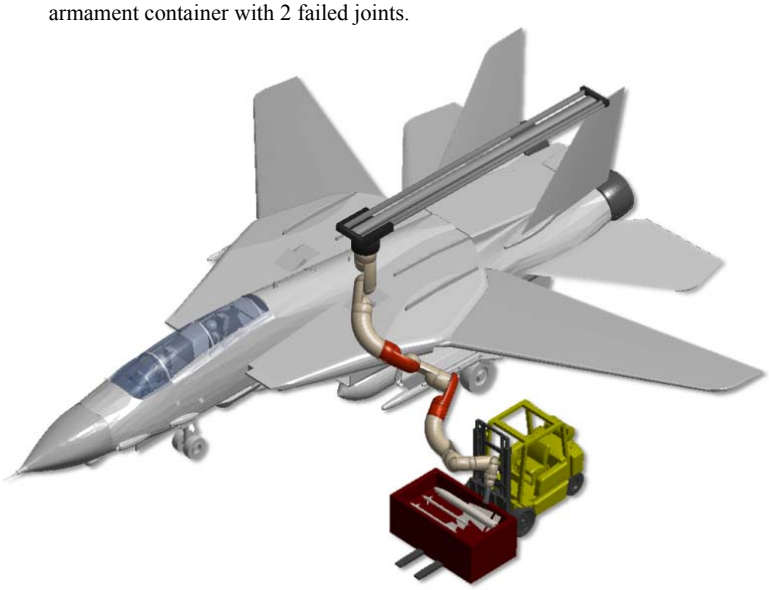

Figure 16 The third-fittest 12DOF 3rd order fault-tolerant manipulator successfully rearming the port-side aircraft wing with 2 failed joints.

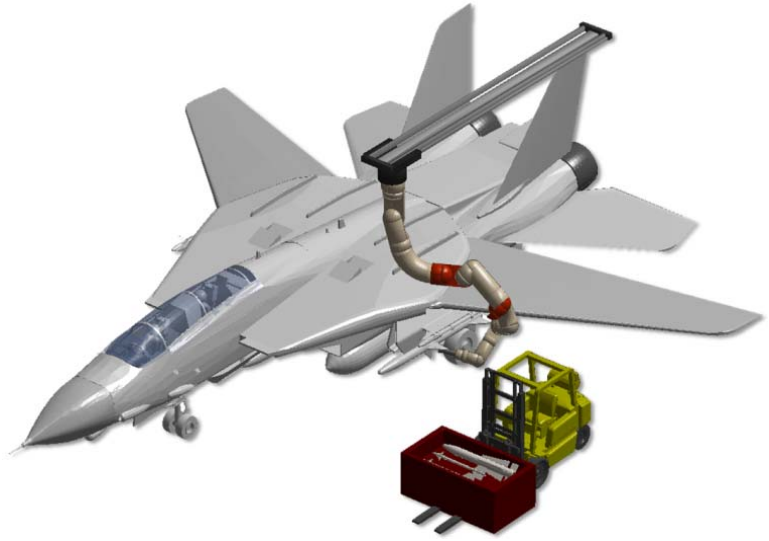

Table 3 Fault-tolerant manipulator design fitness and performance

Manipulator	*RWGII*	*% Dexterity loss*	*MWGII*	*GII*	*Energy (kJ)*
1st Fittest	0.8749	12.5	0.0131	0.0157	285.23
2nd Fittest	0.8726	12.7	0.0118	0.0135	283.76
3rd Fittest	0.8551	14.5	0.0120	0.0118	290.04
139th Fittest	0.5909	41.9	0.0068	0.0074	371.32
140th Fittest	0.5464	45.5	0.0071	0.0052	402.78
141st Fittest	0.5130	48.7	0.0063	0.0068	471.13

Figure 17 A relative morphological comparison between fittest and least fit fault-tolerant manipulator designs. Length is greater and center of mass is more distal than in the least-fit design, which promotes higher torques, and the kinematic isotropy is 41% lower than that of the fittest design.

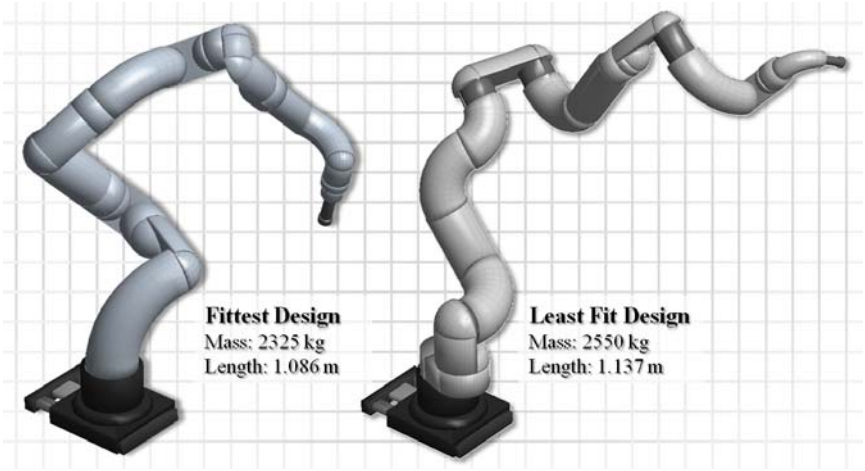

6 Conclusions

This design study demonstrates the efficacy of relative weighted global isotropy index ($RWGII_k$) as a means of designing fault-tolerant kinematically redundant manipulators for use on geometrically complex, mechanically demanding tasks, by designing a 12DOF, 3rd order fault-tolerant manipulator for military aircraft inspection and rearming. The formulation of the $RWGII_k$ heuristically quantifies the ability of the manipulator to maintain kinematic dexterity and multiobjective redundant resolution over two disparate tasks while ensuring a specified level of fault-tolerance capability. $RWGII_k$ improves upon previous global isotropy measures by including all kinematic velocity transmission rates in the calculation of isotropy, not just the extrema, and by considering velocity magnitude. This way, intermittent changes in isotropy along a motion trajectory are not marginalized, and the magnitudes of velocity transmission rates involved in the calculation of isotropy are accounted for.

The results of this work agree with previous weighted-isotropy research results, despite the volume and complexity of the design space and the difficulty in predicting failure-susceptibility. The simulations run for this study, however, are computationally expensive and more stochastic than deterministic in nature. Based on the $RWGII_k$ inflection points observed during GA-optimization and the coincident design parameter changes, future research can be conducted to identify those design parameters which most effect task-specific manipulator design fitness for specialized, secondary functionality, including fault-tolerance. This can lead to a more computationally efficient and robust optimization scheme, and may elucidate a greater understanding of the relationship between manipulator design primitives and performance on demanding tasks.

References

Bryant V. (1993) *Aspects of Combinatorics: A Wide Ranging Introduction*. New York, NY, USA: Cambridge University Press.

Chan, T. and Dubey, R. (1995) 'A weighted least-norm solution based scheme for avoiding jointlimits for redundant joint manipulators,' *Proc. of the 1995 IEEE Trans. on Robotics and Automation*, vol. 11, pp. 286-292.

Caldwell, C. and Roberts, R. (2002) 'Fault-tolerant kinematically redundant robots,' *Proc. of the Thirty-Fourth Southeastern Symp. on System Theory*, Tallahassee, FL, USA, pp. 381-385.

English, J. and Maciejewski, A. (1998) 'Fault tolerance for kinematically redundant manipulators: Anticipating free-swinging joint failures,' *IEEE Trans. on Robotics and Automation*, vol. 14, pp. 566-575.

Gosselin, C. and Angeles, J. (1991) 'A global performance index for the kinematic optimization of robotic manipulators,' *Journal of Mechanical Design*, vol. 113, pp. 220-226, 1991.

Groom, K., Maciejewski, A., and Balakrishnan, V. (1999) 'Real-time failure-tolerant control of kinematically redundant manipulators,' *IEEE Trans. on Robotics and Automation*, vol. 15, pp. 1109-1115.

Hammond III F. and Shimada K. (2009) 'Improvement of Redundant Manipulator Task Agility Using Multiobjective Weighted Isotropy-Based Placement Optimization,' *IEEE Int. Conf. on Robotics and Biomimetics*, Changchun, Jilin, China, pp. 645-652.

Hammond III F., and Shimada K. (2010) 'Multiobjective weighted isotropy measures for the morphological design of kinematically redundant manipulators,' *Int. Jounral of Mechatronics and Manufacturing Systems*.

Khan, W. and Angeles, J. (2006) 'The Kinetostatic Optimization of Robotic Manipulators: The Inverse and the Direct Problems,' *Journal of Mechanical Design*, vol. 128, p. 11.

Kim, J. and Khosla, K. (1991) 'Dexterity measures for design and control of manipulators,' *IEEE/RSJ Int. Workshop on Intelligent Robots and Systems*, Osaka, Japan, pp. 758-763.

Klein, C. and Blaho, B. (1987) 'Dexterity Measures for the Design and Control of Kinematically Redundant Manipulators,' *The Int. Journal of Robotics Research*, vol. 6, p. 72.

Ma, S. (1995) 'A Stabilized Local Torque Optimization Technique for Redundant Manipulators,' *Proc. of the IEEE Int. Conf. on Robotics and Automation*, Nagoya, Japan, pp. 2791-2796.

Maciejewski, A., and Klein, C. (1985) 'Obstacle Avoidance for Kinematically Redundant Manipulators in Dynamically Varying Environments,' *The Int. Journal of Robotics Research*, vol. 4, pp.109-117.

Maciejewski, A. (1990) 'Fault tolerant properties of kinematically redundant manipulators,' *IEEE Int. Conf. of Robotics and Automation*, Cincinnati, OH, USA, pp. 638-642.

Paredis C., Au W., and Khosla P. (1994) 'Kinematic design of fault tolerant manipulators,' *Computers & Electrical Engineering*, vol. 20, pp. 211-220.

Paredis, C. and Khosla, P. (1993) 'Synthesis Methodology for Task Based Reconfiguration of Modular Manipulator Systems,' *6th Int. Symp. on Robotics Research*, Hidden Valley, PA.

Roberts R. and Maciejewski A. (1996) 'A local measure of fault tolerance for kinematically redundant manipulators,' *IEEE Trans. on Robotics and Automation*, vol. 12, pp. 543-554.

Spong, M., Hutchinson , S., and Vidyasagar, M. (2005) *Robot modeling and control*, Hoboken, NJ: John Wiley & Sons, pp. 119-161.

Stocco, L., Salcudean, S., and Sassani, F. (1998) 'Matrix Normalization for Optimal Robot Design,' *IEEE Int. Conf. on Robotics and Automation*, Leuven, Belgium, pp. 1346–1351.

Ting Y., Tosunoglu S., and Fernandez B. (1994) 'Control algorithms for fault-tolerant robots,' *IEEE Int. Conf. on Robotics and Automation*, San Diego, CA, USA, pp. 910-915.

Wampler, C. (1986) 'Manipulator inverse kinematic solutions based on vector formulations and damped least-squares methods,' *IEEE Trans. on Systems, Man, and Cybernetics*, vol. 16, pp. 93-101.

Yoshikawa, T. (1985) 'Manipulability of Robotic Mechanisms,' *The Int. Journal of Robotics Research*, vol. 4, pp. 3-9.